Influence of functional groups on toxicity of carbon nanomaterials

Yongchun Liu [1, 2], Haotian Jiang [2, 4], Chunmei Liu [3], Yanli Ge [2], Lian Wang [2], Bo Zhang [2], Hong He [2, 4,5], Sijin Liu [2, 4]

[1] Aerosol and Haze Laboratory, Advanced Innovation Center for Soft Matter Science and Engineering, Beijing University of Chemical Technology, Beijing, 100029, China

[2] State Key Joint Laboratory of Environment Simulation and Pollution Control, Research Center for Eco-Environmental Sciences, Chinese Academy of Sciences, Beijing, 100085, China

[3] Bioduro Technology (Beijing) Co., Ltd., Beijing, 102200, China

[4] University of Chinese Academy of Sciences, Beijing, 100049, China

[5] Center for Excellence in Urban Atmospheric Environment, Institute of Urban Environment, Chinese Academy of Sciences, Xiamen 361021, China.

Correspondence to: Y. Liu (liuyc@buct.edu.cn) and S. Liu (sjliu@rcees.ac.cn)

Abstract:

It has been well recognized that carbon nanomaterials and soot particles are toxic for human health, while it is still controversial about the influence of functionalization on their toxicity as well as the evolution of the toxicity of carbon nanomaterials due to chemical aging in the atmosphere. In the current study, the oxidation potential measured by dithiothreitol (DTT) decay rate and the cytotoxicity to murine macrophage cells of different functionalized carbon nanomaterials were investigated to understand the role of functionalization in their toxicities. The DTT decay rates of special black 4A (SB4A), graphene, graphene oxide, single wall carbon nanotubes (SWCNT), SWCNT-OH and SWCNT-COOH were 45.9±3.0, 58.5±6.6, 160.7±21.7, 38.9±8.9, 57.0±7.2 and

23 36.7±0.2 pmol $min^{-1}\mu g^{-1}$, respectively. Epoxide was found to be mainly responsible for
24 the largest DTT decay rate of graphene oxide compared with other carbon
25 nanomaterials based on comprehensive characterizations. Both carboxylation and
26 hydroxylation showed little influence on the oxidation potential of carbon
27 nanomaterials, while epoxidation contributes to the enhancement of oxidation potential.
28 All these carbon nanomaterials were toxic to murine J774 cell line. However, oxidized
29 carbon nanomaterials (graphene oxide, SWCNT-OH and SWCNT-COOH) showed
30 weaker cytotoxicity to J774 cell line compared with the corresponding control sample
31 as far as the metabolic activity was considered and stronger cytotoxicity to J774 cell
32 line regarding to the membrane integrity and DNA incorporation. These results imply
33 that epoxidation might enhance the oxidation potential of carbon nanomaterials.
34

1. Introduction

Carbon nanomaterials are predominantly composed of carbon atoms, only one kind of element, but they have largely diverse structures characterized by different degrees of crystallinity and different macro- and micromorphology (Somiya, 2013). Their basic structure is that of graphite with planes of honeycomb-arranged carbon atoms. Carbon black (CB), which is produced from incomplete combustion of heavy petroleum materials under controlled conditions (Apicella et al., 2003), has been widely used in industrial products, such as inkjet printer ink, rubber and plastic products (Lee et al., 2016), electrically conductive plastics (Parant et al., 2017), paints, coatings and cosmetics (Sanders and Peeten, 2011) and so on. CB is a quasi-graphitic form of nearly pure element carbon (EC, consist of graphene layers). It is distinguished by its very low quantities of extractable organic compounds and total inorganics (Long et al., 2013) compared with soot or black carbon (BC) (Andreae and Gelencser, 2006). Soot, which originates from incomplete combustion of biomasses, biofuels, fossil fuels and natural fires in reduced or anoxic environments, is a mixture of elemental carbon and organic carbon (OC) compounds (Muckenhuber and Grothe, 2006). In addition, as a class of engineering nanoparticles, carbon nanotubes (CNTs) and graphene materials are also a large group of carbon nanomaterials although their graphene sheets are arranged more regularly (Hu et al., 2010) than that in CB (Nienow and Roberts, 2006). During production and use of these consumer products, they are prone to enter into the environment and ultimately the human body (Helland et al., 2007;Tiwari and Marr, 2010), subsequently, to pose risk of adverse health effect.

The adverse effect of CB and soot particles on human health has attracted much attention in the atmospheric chemistry community (Baumgartner et al., 2014). Overall, exposure to CB is associated with high risk of cancer, respiratory and cardiovascular diseases (WHO, 2013;Niranjan and Thakur, 2017). Mitochondrial damage in alveolar macrophages and bronchial epithelial cells resulted from exposure of diesel exhaust particles (DEPs) has been observed (Li et al., 2002a;Li et al., 2002b). Oxidation stress or reactive oxygen generation (ROS) is one of mechanisms related to the toxicity of particles including soot particles (Nel et al., 2006), and has been even used as a paradigm to assess particle toxicity (Xia et al., 2006).

Dithiothreitol (DTT) decay rate is commonly used as a cell-free measure of the oxidative potential of different particles (Cho et al., 2005;Charrier and Anastasio, 2012;Kumagai et al., 2002), such as ambient particles (Li et al., 2003;Fang et al., 2016;Cho et al., 2005;Charrier and Anastasio, 2012;Wang et al., 2013), secondary organic aerosol (SOA) (McWhinney et al., 2013b), DEP (Li et al., 2009;McWhinney et al., 2013a), carbon nanotubes (CNT)(Liu et al., 2015), flame soot (Antinolo et al., 2015;Holder et al., 2012;Li et al., 2013) and commercial carbon black (CB) particles (Koike and Kobayashi, 2006;Li et al., 2009;Li et al., 2015;Li et al., 2013). However, the reported DTT decay rate of soot and CB particles varied substantially, from 0.9 to ~50 pmol min^{-1} μg^{-1}. The variation of DTT decay rate among different samples implies the importance of the composition or structure of particles in their toxicities.

Although transition metals, element carbon, humic-like substances and quinones are responsible for ROS generation on particle surface (McWhinney et al., 2013b;Li et

79 al., 2003), more work is still required to deeply understand the toxicity of soot and the
80 reason why the toxicity varies greatly among different soot samples. On the other hand,
81 soot particles are prone to undergo oxidation by O_3, OH and NOx etc. during transport
82 in the atmosphere. Subsequently, functionalization including formation of OH, C=O,
83 epoxide (C-O-C) and COOH occurs (Mawhinney et al., 2000;Liu et al., 2015;Holder et
84 al., 2012;Corbin et al., 2015). This make it more complicate to understand the toxicity
85 of soot particles. For example, several studies have found that atmospheric relevant
86 oxidation of CB or soot by O_3 leads to enhancement of their oxidative potential (Li et
87 al., 2009;Li et al., 2013;Li et al., 2015;Antinolo et al., 2015;Holder et al., 2012). In
88 particular, the DTT decay rate of soot particles has been found increasing as a function
89 of the content of quinone formed via ozone oxidation of organic carbons in soot
90 (Antinolo et al., 2015). However, some other studies have found that oxidation of CB
91 or soot by O_3 or OH under atmospheric related conditions has little influence on their
92 oxidative potential or cytotoxicity although surface functionalization is observable (Liu
93 et al., 2015;Peebles et al., 2011). Therefore, it is necessary to understand the role of
94 functional groups in the toxicity of soot and CB particles.

95 During combustion process, however, multiple functional groups including OH,
96 C=O, COOH, esters, ethers and so on are usually formed at the same time and present
97 in both OC and EC (Han et al., 2012a;Cain et al., 2010;Wal et al., 2011;Popovicheva et
98 al., 2015). Thus, it is difficult to differentiate the role of one kind of functional group
99 from others in the toxicity of soot particles. However, it is possible to investigate the
100 role of functional groups in the toxicity of carbon nanomaterials when using CB or

101 engineered carbon particles with different functional groups as model sample of soot
102 particles. Actually, it has been recognized that the surface properties of carbon
103 nanomaterials will influence their biological effects or toxicity (Lara-Martinez et al.,
104 2017;Liu et al., 2014b;Koromilas et al., 2014). For example, a recent study has found
105 that hydrated graphene oxide exhibited a higher cytotoxicity to THP-1 and BEAS-2B
106 cells as a consequence of lipid peroxidation of the surface membrane and membrane
107 lysis compared to pristine and reduced graphene oxide (Li et al., 2018). Functionalized
108 multiwalled carbon nanotubes (FMWCNTs) is highly cardioembryotoxic in
109 comparison with functionalized oxygen-doped multiwalled carbon nanotubes (Lara-
110 Martinez et al., 2017). As pointed out by Lara-Martinez et al. (2017), however,
111 cytotoxic effects of carbon nanomaterials at the cellular level generate considerable
112 controversy and more research is clearly needed to gain insight into the mechanism of
113 these adverse effects. In addition, passive diffusion and energy-dependent endocytosis
114 are the two methods suggested for particles entry into living cells (Foroozandeh and
115 Aziz, 2018). They can also be distributed to various parts of the body, from where they
116 can either remain, translocate, or be excreted. Therefore, it is meaningful to investigate
117 the influence of functionalization on other endpoints alone even for these carbon
118 nanomaterials.

119 In the current study, both the cell-free toxicity and the cell cytotoxicity of carbon
120 nanomaterials with different functionalities were evaluated to focus on the role of
121 functionalization in their toxicities. DTT decay rate representing the oxidative potential
122 and the cytotoxicity of murine macrophage cell were investigated. The carbon

123 nanomaterials were characterized with inductively coupled plasma-mass spectrometry
124 (ICP-MS), thermal gravity analysis (TGA), X-ray photoelectron spectroscopy (XPS),
125 transmission electron microscopy (TEM) and zeta potential analyzer. The role of
126 oxygen containing species in the toxicity of carbon nanomaterials was discussed. This
127 work will be helpful for understanding the toxicity of carbon nanomaterials with
128 different functional groups.

129 **2. Experimental Section**

130 **2.1 Chemicals and characterization of particle samples.** Commercial carbon
131 nanomaterials including Special Black 4A (SB4A), graphene, graphene oxide, SWCNT,
132 SWCNT-OH and SWCNT-COOH were used in this study. All these functional groups
133 have been identified in soot particles and chemical aged soot or CB particles. SB4A
134 was supplied by Degussa. The other carbon nanomaterials with purity >98% were
135 supplied by Timesnano. To obtain graphene oxide with low epoxide content, graphene
136 oxide was thermally treated at 200 °C for 30 min in high purity (99.999%) nitrogen
137 flow. Dithiothreitol (DTT) was supplied by Sigma-Aldrich. 5,5′-dithiobis-(2-
138 nitrobenzoic acid) (DTNB) was obtained from Alfa Aesar. Standard solutions of metal
139 ions including Cr, Mn, Fe, Co, Ni, Cu, Zn, Cd, As, Sn and Pb were supplied by National
140 Institute of Metrology, China. 30 % H_2O_2 solution was supplied by Sinopharm
141 Chemical Reagent Co., Ltd.

142 A transmission electron microscope (H-7500, Hitachi) was used to investigate the
143 morphologies of carbon nanomaterials (Golberg et al., 2012). Particles were
144 ultrasonically dispersed in ultrapure water (18 MΩ) and a droplet of suspending liquid

was deposited onto a Cu microgrid. An acceleration voltage of 80 kV was used for measurements. The morphologies were shown in Fig. S1. The diameter of primary particles were analyzed by ImageJ 1.41 software (Liu et al., 2010). The diameter of the primary carbon sphere for SB4A was 66±17 nm. The out diameter (OD) of SWCNT, SWCNT-OH and SWCNT-COOH was <2 nm with fiber length of 1-3 μm according to the product report and also confirmed by TEM (Fig. S1). Graphene and graphene oxide were 2-dimensional materials with monolayer and the diameter of 0.5-3 μm.

XPS were measured using an AXIS Supra/Ultra (Kratos, Kratos Analytical Ltd.) to identify the oxygen containing species on the surface of carbon nanomaterials (Wal et al., 2011;Schuster et al., 2011). The samples were excited by Al Kα X-ray ($h\nu$=1486.7 eV) with 15 kV of working voltage and 40 mA of emission current. The spectra were analyzed with XPS Peak software. The content of organic carbon (OC) in carbon nanomaterials was measured by thermal desorption using a commercial TG instrument (TGA/DSC1/HT1600, Mettler-Toledo Co., Ltd.). The amount of OC lost from the particles was recorded when the temperature was ramped from 30 to 300 °C at 10 °C min^{-1} in nitrogen flow according to the protocol reported in previous work (Han et al., 2012a). Metals in the particles were measured with an inductively coupled plasma mass spectrometer (ICP-MS 7500a, Agilent Technologies) after digested with concentrated 1:3 HNO_3/HCl. Transition metals were quantified with the standard solution. Zeta potentials of the carbon nanomaterials were measured after sonicating for 30 min in ultrapure water (18.2 MΩ) by using a Nanoparticle Size & Zeta Potential Analyzer (Zetasizer Nano, ZS90).

2.2 DTT assay test. The DTT assay is an indirect chemical assay used for measuring the redox cycling capacity of PM (Xia et al., 2006). The added DTT is oxidized to its disulfide form by the ROS in particulate matter (Kumagai et al., 2002). Thus, the rate of DTT consumption is proportional to the concentration of the ROS in the sample (Cho et al., 2005). In this study, ~150 μg carbon nanomaterials were suspended in 10.0 ml phosphate buffer (0.1 M, pH 7.4) and sonicated for 15 min. 2.0 ml of 0.5 mM DTT solution was added to 3.0 ml aliquots of the sonicated suspensions. A redox reaction took place in a thermostat shaking chamber at 37 ºC. The remained DTT concentration was measured every 15 minutes by adding 0.25 ml of the reaction mixture filtration to 1.0 ml of 0.25 mM DTNB solution. DTNB reacted with the thiol groups in DTT to form a yellow compound (2-nitro-5-thiobenzoate, NTB), which could be detected by UV-vis absorption spectrometer (723N, Shanghai Ruiting Technology Co., Ltd) at 412 nm. Then, the amount of DTT consumed by PM was calculated according to the standard curves of DTT. The loss rate of DTT via a redox reaction in the presence of PM was monitored as the decrease of DTT concentration and normalized to the particle mass. Blank experiments were carried out without carbon nanomaterial particles in the buffer solution. For some samples, the response to the DTT assay was also measured for the water-soluble components of SWCNT by filtering aliquots of the samples with a 0.22 μm syringe PTFE filter, and measuring the activity of the solution without particles.

2.3 In vitro assays. Carbon nanomaterial particles were dispersed with 0.025% Tween-80 in 0.19% NaCl solution using a Dounce glass homogenizer, followed by sonication. A homogeneous and stable suspension of SWCNTs was obtained after the sonication

process. Cytotoxicity assessment of carbon nanomaterials was carried out using the murine J774 cells. Three different assays targeting distinct mechanisms of cellular metabolic perturbations were assessed simultaneously, including ATP (energy metabolism), LDH (membrane integrity) and BrdU (incorporation into DNA) assays. The experiments were carried out according to the corresponding protocol. Briefly, 4×10^5 J774 cells ml^{-1} were exposed to carbon particles in 96-well plates for 24 hours for ATP and LDH assays, while the initial J774 cell concentration was 2×10^5 cells ml^{-1} for BrdU assay. Carbon nanomaterials were dosed at 0, 10, 30 and 100 μg cm^{-2} in a final volume of 200 μl $well^{-1}$ as similar to that reported in literatures (Kumarathasan et al., 2014;Kumarathasan et al., 2012). The luminescence spectroscopy of the supernatant after centrifugal separation at 1000 rpm for 5 min was measured after 24 h of cell exposure using a Multimode Microplate Reader (Varioskan®Flash, Thermo Fisher Scientific). The zero dose of carbon nanomaterials referred to the blank experiment and also means the toxicity of 0.025% Tween-80 alone in 0.19% NaCl solution. Similar to the literature results (Hadrup et al., 2017), they did not incur any obvious deleterious effect on cells growth. In addition, it has been well recognized that carbon nanoparticles tended to aggregate in water even after ultrasonic dispersion. Tween-80 has been verified to be a biocompatible dispersant for carbon black (Kim et al., 2012). Negative control experiments were performed in wells containing medium without cells to obtain a value for background luminescence. Positive control experiments were carried out with H_2O_2 solution for LDH assays (Fig. S2).

3. Results

3.1 Oxidative potential of carbon nanomaterials. Figure 1 shows the DTT decay rates of SB4A, graphene, graphene oxide, SWCNT, SWCNT-OH and SWCNT-COOH. They were 45.9±3.0, 58.5±6.6, 160.7.0±21.7, 38.9±8.9, 57.0±7.2 and 36.7±0.2 pmol $min^{-1}\mu g^{-1}$, respectively. Except for graphene oxide, the measured DTT decay rates for these carbon nanomaterials (with mean value of 47.4±10.1 pmol $min^{-1}\mu g^{-1}$) were comparable with the DTT loss rates of soot reported in the literatures. For example, it was 36.2±4.9 pmol min^{-1} μg^{-1} for Printex U (Li et al., 2015) and 59.3±7.4 pmol min^{-1} for typical soot particles, such as 33.6 pmol min^{-1} μg^{-1} for methane flame soot (Holder et al., 2012), 49±7 pmol min^{-1} μg^{-1} for propane flame soot (Antinolo et al., 2015), 27.0 pmol min^{-1} μg^{-1} for hexane flame soot (Li et al., 2013), as well as the typical ambient $PM_{2.5}$ particles (34.7±19.1 pmol min^{-1} μg^{-1}) (Charrier and Anastasio, 2012;Liu et al., 2014a). However, the measured DTT decay rates for these carbon nanomaterials were significantly higher than that of diesel soot (6.1 pmol min^{-1} μg^{-1}) and graphite (0.9 pmol min^{-1} μg^{-1}) (Li et al., 2013) reported in previous work. It should be noted that the DTT decay rate of graphene oxide measured in this study was 160.7±21.7 pmol min^{-1} μg^{-1}. Based on T-test, the DTT decay rate of graphene oxide was significantly higher than that of other tested carbon nanomaterials at the 0.05 level (t=8.498, which is greater than the critical value of 2.447). This means that graphene oxide definitely has a stronger oxidative potential than other CB or carbon nanomaterials in this work.

3.2 Cytotoxicity of carbon nanomaterials to murine J774 cell line. At the present time, the A549 (a human adenocarcinomia alveolar epithelial cell) and THP-1 (a human leukemia monocytic cell line) cell lines were usually chosen as target cell lines

(Kumarathasan et al., 2012;Kumarathasan et al., 2014;Liu et al., 2015) to evaluate the alveolar and pulmonary toxicity of CB particles. As the first barrier of the immune system, macrophage cell lines will fight against the invaded particles in the lungs. Macrophage cell lines like J774 cells are ideal model systems for establishing the biophysical foundations of autonomous deformation and motility of immune cells (Lam et al., 2009). It has been found that CB nanoparticles are able to stimulate the release of macrophage chemo-attractants when exposed to type II epithelial cell lines (L-2 cells) at sub-toxic doses (Barlow et al., 2005). CNTs exposure can also lead to biological changes in J774 cells (Kumarathasan et al., 2012). Therefore, it is meaningful to investigate the cytotoxicity of different carbon nanomaterials as well as the influence of surface functional group on the macrophage cell lines.

Figure 2 shows the in vitro toxicities of SB4A, graphene, graphene oxide, SWCNT, SWCNT-COOH and SWCNT-OH. The stars mean the indicator of the toxicity at a certain dose of carbon nanomaterials is significantly different from the corresponding blank experiments at 0.05 level. As shown in Fig. 2, the metabolic activity of J774 cell line decreased monotonously as a function of the dose of all these carbon nanomaterials. The relative ATP level (1.01±0.02) at the SB4A dose of 10 μg cm^{-2} was almost the same as that of the blank sample, while it significantly decreased to 0.89±0.05 and 0.61±0.07 when the dose of SB4A increased to 30 μg cm^{-2} and 100 μg cm^{-2}, respectively. Similarly, the relative ratio of BrdU incorporation decreased from 0.74±0.03 to 0.60±0.04 when the dose of SB4A increased from 30 to 100 μg cm^{-2}. However, the released LDH levels were constant within experiment uncertainty at different SB4A doses.

As shown in Fig. 2B-F, the metabolic activity of murine J774 cell decreased more significantly when exposed to engineered carbon nanomaterials than SB4A. For example, the relative ratio of ATP level was 0.67±0.06, 0.84±0.03, 0.59±0.10, 0.93±0.01 and 0.88±0.02 even when the J774 cells were exposed to 10 μg cm^{-2} graphene, graphene oxide, SWCNT, SWCNT-OH and SWCNT-COOH, respectively. When exposed to high doses of engineered carbon nanomaterials, the reduction of relative ATP level became more significant. These results mean the cytotoxicity of the engineered carbon nanomaterials studied in this work are stronger than that of SB4A regarding to metabolic activity. Graphene, graphene oxide and SWCNT-COOH significantly enhanced release of LDH at different exposure levels, while SWCNT and SWCNT-OH only led to significant increases of released LDH at high exposure level (100 μg cm^{-2}).

It should be noted that the reduction of ATP ratio of J774 cells exposed to graphene oxide was weaker than that of graphene. The reduction of ATP ratio of J774 cells exposed to SWCNT-OH or SWCNT-COOH was also weaker than that of SWCNT. However, compared with graphene, graphene oxide showed much stronger toxicity to J774 cell as far as the membrane integrity was considered. The released LDH at exposure level of 30 μg cm^{-2} graphene oxide was comparable with that when exposed to 150 ppm H_2O_2 (Fig. S2). In addition, graphene oxide, SWCNT-OH and SWCNT-COOH significantly inhibited DNA synthesis of J774 cells when the carbon nanomaterials doses were above 10 μg cm^{-2}, while graphene and SWCNT did not show significant inhibition of DNA synthesis for J774 cells. For instance, the relative ratio of

277 BrdU when J774 cells exposed to 100 μg cm^{-2} of graphene oxide was 0.61±0.10, while
278 it was 0.77±0.10 for graphene exposed cells at the same exposure level. They were
279 0.62±0.10 for SWCNT-OH and 0.56±0.09 for SWCNT-COOH treated cell at a dose of
280 10 μg cm^{-2} compared with 0.83±0.09 for 10 μg cm^{-2} of SWCNT treated J774 cell.
281 **3.3 Characterization of carbon nanomaterials.** As shown in Fig. S1, the
282 morphologies of these carbon nanomaterials varied greatly. SB4A was a zero-
283 dimensional material. SWCNT, SWCNT-OH and SWCNT-COOH were one
284 dimensional material. Graphene and graphene oxide were two dimensional materials.
285 The content of transition metals including Cr, Fe, Mn, Co, Ni, Cu, Zn, As, Cd, Sn
286 and Pb were measured by using an ICP-MS after the carbon nanomaterials were
287 digested with 1:3 HNO_3/HCl. As shown in Fig. S4A, Fe was the most abundant
288 transition metal in these carbon nanomaterials. Its concentration varied from 122 μg g^{-1}
289 to 6596 μg g^{-1} among different carbon nanomaterials. The concentration of other
290 metals varied from zero to several hundred μg g^{-1} depending on both carbon
291 nanomaterials and the type of metals. Compared with SB4A, these engineered carbon
292 nanomaterials showed higher metal content. For example, the total metal content in
293 graphene was 6 times as high as that in SB4A, while it was 33 times in SWCNT as high
294 as that in SB4A. This can be explained by the fact that graphene and SWCNT materials
295 were catalytically synthetized using metal catalysts containing Fe, Co or Ni (Maruyama,
296 2018).
297 Figure 3 shows the thermo gravity and differential thermal analysis curves for these
298 CB materials when the temperature was ramped from 30 to 300 °C at 10 °C min^{-1} in

299 nitrogen flow. Weight loss (Fig. 3A) accompanied with an endothermic process (Fig.
300 3B) were observed below 60°C for all of these samples. This can be ascribed to
301 desorption of surface adsorbents including bonded organics and trace water. As shown
302 in Fig. 3B, the saddle points of these differential thermal analysis curves were observed
303 at 35, 35, 41, 42, 56 and 58 °C for graphene, SWCNT, SB4A, SWCNT-OH, SWCNT-
304 COOH and graphene oxide, respectively. It should be noted that the oxidized carbon
305 nanomaterials such as SWCNT-OH, SWCNT-COOH and graphene oxide showed
306 higher saddle points of the heat curves than graphene, SWCNT and SB4A. This implies
307 stronger interaction between the adsorbents and these three oxidized carbon
308 nanomaterials compared with the counterpart. Therefore, it is reasonable to deduce that
309 the adsorbed water mainly contributes to the weight loss in this stage. The sample
310 weight slightly decreased as the temperature further increased for all of these carbon
311 nanomaterials except for graphene oxide and accompanied with a gradual increase of
312 the heat flow. This can be ascribed to desorption of adsorbed organics from the surface
313 of the carbon nanomaterials. The relatively small increase rate of the heat in this stage
314 was consistent with the small heat capacity of organics when compared with the first
315 one which was ascribed to desorption of water. For graphene oxide, however, weight
316 loss (from 32% to 60%) was significantly observed accompanied with an acute
317 exothermic process when the temperature increased from 150 to 200 °C as shown in
318 Fig. 3B. This implies that release of pyrolysis products and structure collapse of
319 graphene oxide occur. It also means a high reactivity of graphene oxide and highlights
320 the distinctive property of graphene oxide among these investigated carbon

nanomaterials. The adsorbed organics were estimated based on the thermogravimetric curves when the possible contribution of water was ruled out. For graphene oxide, 150 °C was taken as the endpoint, while 300 °C was chosen for other samples. The content of adsorbed organics on SB4A, graphene, graphene oxide, SWCNT, SWCNT-OH and SWCNT-COOH was 6 %, 13 %, 15 %, 9 %, 5 % and 9 %, respectively.

To further investigate the role of surface oxygen in the toxicity of carbon nanomaterials, the oxygen-containing species of these carbon nanomaterials were identified with X-ray photoelectron spectroscopy. Fig. 4 shows the typical O1s and C1s spectra of these carbon nanomaterials. Several oxygen-containing species were observed as shown in Fig. 4A-F. Adsorbed oxygen was observed at 535.2 eV in the O1s spectra. Carbon-oxygen single bond in hydroxyl group (C-OH) and epoxide (C-O-C) were at 533.5 and 532.6 eV, respectively. Carbon-oxygen double bound (C=O) was observed at 531.8 eV, while highly conjugated form of carbonyl oxygen such as quinone groups was identified at 530.5 eV (Schuster et al., 2011). In the C1s spectra (Fig. 4G-L), the band at 291 eV was attributed to the shakeup peak associated with π-π* transition (Simmons et al., 2006). The band at 289 eV corresponded to carbonyls and epoxides was observed at 287 eV (Kuznetsova et al., 2001). The band at 285 eV and 284.6 eV was assigned to graphite and sp^3 carbon, respectively. In particular, the intensity of C-O-C at 532.6 eV in graphene oxide was very strong compared with other carbon nanomaterials. At the same time, the band of C-O-C at 287 eV was also much stronger than that of other carbon nanomaterials in the C1s spectrum. These results mean that epoxides (C-O-C) is the predominating species (Fig. 5C and I) in graphene

343 oxide. It should be noted that XPS results only represent the surface atom ratios, which
344 are different from the OC content representing the bulk composition. However, the
345 surface property of particle should be very important to understand the toxicity of
346 nanoparticles from the point view of particle-cell interaction (Cedervall et al., 2007).

347 **4. Discussion**

348 As shown in Fig. 2, all the carbon nanomaterials showed decreased ATP activities
349 as a function of the dose. This means the carbon nanomaterials investigated in this work
350 are toxic to murine J774 cell line. This is consistent with the previous results that CNT
351 and Printex U are toxic to J774 cells (Kumarathasan et al., 2012) and graphene oxide
352 can induce dose-dependent cell death in normal lung fibroblasts (HLF), macrophages
353 (THP-1 and J744A), epithelial (BEAS-2B) cells, lung cancer cells (A549) etc. (Zhang
354 et al., 2016;Li et al., 2018). At the same time, the BrdU activities decreased as a function
355 of the dose of carbon nanomaterials, which means they are inhibitor for cell
356 proliferation of murine J744 (Cappella et al., 2015). In addition, except for SB4A, other
357 carbon nanomaterials showed significant increases in LDH. This means that the
358 integrity of cell membrane decreased when J774 cells were exposed to these engineered
359 carbon nanomaterials, while the cell membrane might be intact when exposed to SB4A
360 (Cho et al., 2008;Kumarathasan et al., 2015). This might be related to lipid peroxidation
361 induced by these engineered particles (Li et al., 2018) and the non-sphere feature of
362 these engineered particles as observed in Fig.S1. These results also consistent with the
363 previous study that observed CNT cytotoxicity ranking was assay-dependent
364 (Kumarathasan et al., 2015).

As shown in Fig. S3, all these carbon nanomaterials revealed negative zeta potential from -42 mV to -20 mV. SB4A, graphene oxide and SWCNT-COOH almost borne the same zeta potential (-42 mV), while SWCNT, SWCNT-OH and graphene showed comparable zeta potential. This observation suggested the stability of dispersed SB4A, graphene oxide and SWCNT-COOH in water and the interaction between these particles with cells was comparable. However, the cytotoxicity of SB4A, graphene and SWCNT showed an increase trend regarding the metabolic activity of J774 cell (Fig. 2). This can be explained by the different mode of action (MOA) when the cells were exposed to different types of nanomaterials. For example, adhesions and/or covering on cells could be the main MOA for graphene/graphene oxide (2-D structure) (Gupta et al., 2019;Keshavan et al., 2017), while for carbon nanotubes (1-D structure), piercing and/or internalization by cells could be the main MOA (Lacerda et al., 2013). This means morphology should plays a role in determining the cytotoxicity of the carbon nanomaterials studied in this work. Therefore, in the following section we mainly discuss the cytotoxicity among these materials having same dimension, such as SWCNT-OH and SWCNT-COOH verse SWCNT and graphene oxide verse graphene.

It should be noted that oxidized carbon nanomaterials including graphene oxide, SWCNT-OH and SWCNT-COOH showed weaker reduction of ATP ratio of J774 cells than the counterparts (Fig. 2). These results suggested that functionalized carbon nanomaterials caused a low cytotoxicity of murine J774 cell line regarding to the cell apoptosis, while a stronger toxicity was demonstrated for cell proliferation and the membrane integrity. This finding was true, in particular, for graphene oxide. However,

387 we did not observe a clear dependence of cytotoxicity to murine J774 cell line on the
388 morphology, the transition metal content, the OC content and the content of oxygen-
389 containing species on the surface of carbon nanomaterials although oxidized CB
390 materials showed reduced toxicity to J774 cell lines as far as metabolic activity was
391 considered. In particular, the difference in surface oxygen content between graphene
392 oxide and graphene was much higher than that between SWCNT-OH/SWCNT-COOH
393 and SWCNT (Fig. 5A), while the differences in metabolic activity to J774 cell line
394 between graphene oxide and graphene was similar to that between SWCNT-
395 OH/SWCNT-COOH and SWCNT. The pathways of cellular toxicity induced by
396 particles reside in both oxidative stress (ROS) and non-oxidative stress dependent
397 (Shvedova et al., 2012). Oxidative stress leads to selective oxidation of mitochondrial
398 CL, NADPH oxidase activation and MPO activation in neutrophils, while non-
399 oxidative stress results from interference with mitotic spindle and actin cytoskeleton,
400 and steric hindrance of ion channels. The interaction between target cells and particles
401 should be much complicated than that between DTT and particles. As discussed above,
402 the cytotoxicity of nanoparticles relied on not only the mode of action but also the
403 chemical nature of particles. Therefore, the different responses of the oxidation
404 potential and the cytotoxicity to the epoxide content in these carbon materials might be
405 accounted for by different mechanisms of toxicity among these assays.

406 The DTT decay rate (Fig. 1) did not show obvious dependence on their
407 morphologies in this work. For example, except for graphene oxide, the DTT decay
408 rates were comparable among all the other materials regardless of the morphology.

Graphene and graphene oxide showed similar particle size, graphene layer and morphologies (Fig. S1), while they showed totally different toxicity as shown in Fig. 1. Transition metals in the particles have been identified to be the important contributor to ROS generation (McWhinney et al., 2013b;Li et al., 2003). It should be noted that although the metal content of SB4A was very low compared with other materials (Fig. S4), the DTT decay rate of SB4A was still comparable with these engineered carbon nanomaterials except for graphene oxide as shown in Fig. 1. On the other hand, SWCNT had the highest metal content, while graphene oxide rather than SWCNT showed the strongest DTT decay rate. In addition, the soluble metal contents were in the following order: SWCNT-COOH > SWCNT > SB4A > graphene oxide > graphene > SWCNT-OH (Fig. S4B), after being sonicated for 30 min in water. Graphene oxide (103.7 μg g^{-1}) did not show a significant difference compared with SB4A (106.3 μg g^{-1}) and graphene (93.7μg g^{-1}). These results indicated that the high oxidative potential of graphene oxide relative to other materials cannot be attributed to their difference in bounded or soluble transition metals. This can be explained by the following reasons. First, metal content was measured after digested with 1:3 HNO_3/HCl. The speciation of metals should be quite different from that presenting in the pristine carbon nanomaterials. For example, the contents of soluble metal ions after sonicated for 30 min (Fig. S4B) varied from zero to 356 μg g^{-1}. These values were much lower than the corresponding metal contents of digested samples as shown in Fig. S4A. Second, metal might be in the inner pores of carbon nanomaterials. This will decrease the efficiency of metals to generate ROS. Finally, the concentration of carbon nanomaterials was 10-

40 μg ml^{-1} in DTT assay tests. This meant the concentration of transition metals was at ng ml^{-1} level even if all of the transition metals were available. The low concentration of metals released might lead to negligible contribution to ROS formation. This was further confirmed by the very small DTT decay rate of the SWCNT filtered solution (1.66±0.15 pmol min^{-1} μg^{-1}) compared with that of SWCNT suspension (38.9±8.9 pmol min^{-1} μg^{-1}) even though SWCNT had the highest metal concentration (Fig. S4A). This was consistent with the previous conclusions that redox activity originates from the surface of CB or soot particles but not from water-soluble substances (Liu et al., 2015;McWhinney et al., 2013a).

As shown in the insert graph of Fig. 3A, the content of organics cannot explain the sequence of the DTT loss rate (Fig. 1) of these carbon nanomaterials. For example, the content of organics on graphene and graphene oxide were almost the same, while the DTT decay rate of graphene oxide was as about 2.5 times as that of graphene (Fig. 1) This means the different DTT loss rate observed in this study cannot be explained by the adsorbed organics among these materials. Fig. 5A summarizes the distribution of the oxygen species mentioned above normalized to O atoms in these carbon nanomaterials. At the present time, the relative sensitivity factors for each oxygen-containing species are unavailable. Similar to the method used in the literatures (Chen et al., 2017;Schuster et al., 2011), we simply assumed all these oxygen-containing species in the envelope of O1s having the same relative sensitivity factors. It should be reliable when semi-quantitatively comparing the contents of oxygen-containing species among different samples although additional uncertainties might be introduced for the

calculated oxygen content. Highly conjugated form of carbonyl oxygen (quinone) and adsorbed oxygen contributed little to the total oxygen on the surface (<1 %), while C=O, C-O-C and C-OH were predominating oxygen-containing species. Our results agree well with the previous work that C=O, C-O-C and C-OH dominated oxygen-containing species on natural chars, diesel soot, hexane soot and activated charcoal (Langley et al., 2006). Although quinone has been well recognized to contribute to ROS generation on the surface of fine particles (Kumagai et al., 2002;Li et al., 2002b), the content of quinone was lower than 0.35% and showed little difference among all of these tested carbon nanomaterials (Fig. 5A and B). It did so for adsorbed oxygen content. Therefore, we can conclude that the very large DTT decay rates of graphene oxide compared with other carbon nanomaterials as shown in Fig. 5C cannot be explained by the content of quinone or adsorbed oxygen.

As shown in Fig. 5A, the total oxygen content of SB4A, graphene, SWCNT, SWCNT-OH and SWCNT-COOH was 6.68%, 2.41 %, 2.88%, 3.60% and 9.21%, respectively. They were comparable with that of diesel soot (2.1%-12.2%) (Schuster et al., 2011). However, the oxygen content of graphene oxide (29.0%) was significantly higher than the other carbon nanomaterials (Fig. 5A). At the same time, the distribution pattern of the surface species on graphene oxide was quite different from the other carbon nanomaterials. Fig. 5B compared the content of the oxygen-containing species of graphene oxide with other carbon nanomaterials. The red stars indicate the content of oxygen-containing species in graphene oxide, while the blue boxes show that of other carbon nanomaterials. It can be seen that the content of quinone and adsorbed oxygen

showed no difference between graphene oxide and other carbon nanomaterials. The concentration of C=O and C-OH in graphene oxide was slightly higher than that in the other carbon nanomaterials. However, the content of epoxide in graphene oxide was significantly higher than the other carbon nanomaterials. The content of epoxide in graphene oxide normalized to O atoms was 20.8 %, which was 71.7 % of its total oxygen content (Fig. 5B), while it was less than 2.7 % in other carbon nanomaterials. This well corresponded to the large DTT decay rates of graphene oxide (160.7 pmol min^{-1} μg^{-1}) compared to other carbon nanomaterials (less than 60 pmol min^{-1} μg^{-1}) as shown in Fig. 5C. It should be noted that the content of epoxide was not linearly correlated to the DTT activity. This can be explained by the typical nonlinear relationship between the dose of toxicant and toxicity (Antinolo et al., 2015). It should be pointed out that multiple parameters of particle may have influence on its toxicity, in particular, on the cytotoxicity. For example, particle size and morphology may have influence on the material mobility and uptake by cells. Although the observed toxicity including DTT activity and cytotoxicity could be a coincidence of the chemical composition, functional groups and morphology of these particles, the above results at least imply that these physiochemical properties such as morphology, metal and OC content should not be crucial factors as for the toxicity of these carbon nanomaterials because it is difficult to observe an obvious dependence of the toxicity on these factors. In the meantime, we can propose that epoxides in graphene oxide are mainly responsible for the high ROS activity of graphene oxide. The high ROS formation potential of graphene oxide might also explain its strong cytotoxicity to J774 cell line

497 regarding to the cell membrane.

498 To further confirm this assumption, we measured the ROS activity of the thermally
499 treated graphene oxide at 200 °C in nitrogen flow because the C-O-C (epoxide)
500 structure can be broken under this condition as shown in Fig. 3 and discussed above.
501 XPS spectra confirmed the broken of epoxide by the fact that the content of epoxide in
502 thermally treated graphene oxide decreased to 4.3% from 20.9% in graphene oxide as
503 shown in Figs. S5 and S6. In addition, TEM results also showed that graphene oxide
504 broke into small sheets, whose morphology and particle size were close to that of SB4A
505 (Fig. S1). At the same time, the DTT decay rate of the thermally treated graphene oxide
506 decreased to 54.9±9.8 pmol min^{-1} μg^{-1} (Fig. 6). This value was comparable to the DTT
507 decay rates of other carbon nanomaterials, in particular, graphene (58.5±6.6 pmol min^{-1}
508 μg^{-1}) (Fig. 1), while it was significantly lower than the graphene oxide (160.7.0±21.7
509 pmol min^{-1} μg^{-1}) as shown in Fig. 6. It should be noted the total oxygen contents of
510 thermally treated graphene oxide was 19.3 %, which was lower than that of graphene
511 oxide (29.0 %) but significantly higher than that of other carbon nanomaterials.
512 However, the DTT decay rate of thermally treated graphene oxide was still comparable
513 with other carbon nanomaterials. This further highlights the importance of functional
514 group in the DTT decay rate. Therefore, it means that epoxides in graphene oxide are
515 the highly reactive site for ROS formation on the surface of graphene oxide. This is for
516 the first time to observe that epoxide is a highly reactive site for ROS formation besides
517 quinone on carbon nanomaterials. This result is also well consistent with the previous
518 founding that epoxides in graphene oxide can oxidize SO_2 to sulfate (He and He, 2016)

519 although their oxidation mechanism might be different.

520 It should be noted that if other ethers present in the carbon nanomaterials, they
521 should also contribute to the O1s band which might be closed to that of epoxide.
522 However, at the present time, it has been recognized that oxygen-containing species
523 including epoxide, hydroxyl, carbonyl and carboxylic groups present in graphene layer
524 (Inagaki and Kang, 2014;Hunt et al., 2012). Epoxide should dominate the band at 532.6
525 eV compared with ethers (Hunt et al., 2012). In particular, the TGA results also
526 supported the high content of epoxide in graphene oxide. For other samples in this work,
527 other ethers might overestimate their contents of epoxide. However, this should not
528 have influence on our conclusion that epoxides are related to the high oxidation
529 potential of graphene oxide.

530 Recently, environmentally persistent free radicals (EPFRs) (a kind of surface
531 stabilized metal-radical complexes characterized by an oxygen-centered radical)
532 (Dugas et al., 2016) have been identified in different source of particles including
533 biomass/coal combustion, diesel and gasoline exhaust, ambient $PM_{2.5}$ and polymer
534 (Balakrishna et al., 2009;Truong et al., 2010;Dugas et al., 2016). However, it is unclear
535 that whether epoxide in graphene oxide observed in this study contributes to the EPFRs
536 formation. This is needed to be investigated in the future.

537 **5. Conclusion and atmospheric implications**

538 Oxidation is a useful method to obtain functionalized CB materials with distinctive
539 performance in industry. This process unusually leads to formation of carbonyls,
540 hydroxyls, carboxylic acids, esters, ethers and epoxides on the surface of CB or soot

541 particles. Previous work have found that oxidation of carbon nanomaterials (SWCNT)
542 by O_3 or OH under atmospheric related conditions has little influence on their oxidative
543 potential or cytotoxicity although carbonyls, carboxylic acids and esters were formed
544 (Liu et al., 2015). Similarly, surface functionalization was observed for commercial CB
545 materials by ozone oxidation, while increase in the cytotoxicity of murine macrophages
546 and release of inflammation markers upon exposure to the oxidized CB were not
547 observed (Peebles et al., 2011). However, some other studies observed that oxidation
548 process enhanced the oxidation potential (Li et al., 2015;Li et al., 2013;Antinolo et al.,
549 2015) as well as the cytotoxicity (Holder et al., 2012) of CB and soot particles. Using
550 the model carbon nanomaterials with different dominate surface functionalities in this
551 work, we have found that hydroxyl and carboxyl functionalized CB particles had little
552 influence on their oxidation potential, while epoxide functionalized CB (graphene
553 oxide) led to a very strong oxidation potential. Epoxide has been identified as a surface
554 product on SWCNT when treated with high concentration of ozone (Mawhinney et al.,
555 2000;Yim and Johnson, 2009). Besides carboxylic acids, esters (Liu et al., 2015),
556 ketone, lactone and anhydride species (Liu et al., 2010;Han et al., 2012b), epoxides has
557 also been identified as the surface product during oxidation of SWCNT in atmosphere
558 relevant conditions (Liu et al., 2015). On the other hand, graphene oxide was an
559 important commercial product, while showed strong oxidation potential as observed in
560 this work. This means that exposure to epoxide-containing carbon materials should lead
561 to high health risk regarding to oxidation potential. Therefore, Mussel-inspired
562 chemistry is necessary for fabrication of functional materials and decreasing their

563 toxicity and for biomedical applications (Liu et al., 2014b;Zhang et al., 2012).

564 It has been found that CB particles (Printex 90) can induce opening of plasma
565 membrane calcium channels leading to a calcium influx and cause significant release
566 of proinflammatory cytokine TNF-α by the murine J774 cells (Brown et al., 2004),
567 subsequently potentially induce migration of macrophages (Barlow et al., 2005). This
568 could initiate the recruitment of inflammatory cells to sites of particle deposition and
569 the subsequent removal of the particles by macrophages. The metabolic activity of these
570 hydroxyl, carboxylic acid and epoxide functionalized carbon nanomaterials increased
571 when compared with the corresponding sample as observed in this work. This implies
572 functionalization of carbon nanomaterials might not pose an enhanced cytotoxicity risk
573 to macrophages compared with the corresponding control materials although the
574 oxidized carbon nanomaterials were still toxic as far as metabolic activity was
575 considered. However, the oxidized carbon nanomaterials might pose enhanced
576 cytotoxicity to macrophages regarding to membrane integrity and DNA synthesis. It
577 should be pointed out that exposure experiments were performed under high particle
578 concentration with short exposure time in this work. More work needs to be done at
579 low particle concentration with long exposure time in the future. On the other hand, the
580 interaction between particles and biological entities such as proteins or cells has not
581 been considered in this work. Therefore, the in vivo toxicological effect of these
582 functionalized particles needs to be further evaluated in the future. Finally,
583 condensation of co-emitted species and photo oxidation products is particularly rapid
584 under conditions of soot emissions (Johnson et al., 2005;Adachi et al., 2010;Peng et al.,

2016). In previous our work, it has been found that condensation process significantly decreased the oxidation potential of the SWCNTs (Liu et al., 2015). A recent work has also found that condensation of organic aerosol leads to decrease in oxidation potential of engineered nanoparticles (Liu et al., 2019). Therefore, the contribution of functional groups to the oxidation potential should be greatly influenced by condensation of co-emitted species and photo oxidation products in the atmosphere. This might be dependent on the carbon nanomaterial itself and needs to be investigated in the future.

Data availability. The experimental data are available upon request to the corresponding authors.

Supplement. The supplement related to this article is available online at:

AUTHOR INFORMATION

Author contributions. YL, HH and SL designed the experiments. YL wrote the paper. YL, HJ and YG did the DTT assay tests. CL and LW did the cytotoxicity assessments. HJ and BZ performed the characterization of samples.

ACKNOWLEDGMENTS

This research was financially supported by the National Natural Science Foundation of China (48177306 and 91543109) and the Fundamental Research Funds for the Central Universities (PT1907). YL should thank Beijing University of Chemical Technology

for financial supporting.

References:

Adachi, K., Chung, S. H., and Buseck, P. R.: Shapes of soot aerosol particles and implications for their effects on climate, Journal of Geophysical Research-Atmospheres, 115, 9, 10.1029/2009jd012868, 2010.

Andreae, M. O., and Gelencser, A.: Black carbon or brown carbon? The nature of light-absorbing carbonaceous aerosols, Atmos. Chem. Phys., 6, 3131-3148, doi: 10.5194/acp-6-3131-2006, 2006.

Antinolo, M., Willis, M. D., Zhou, S., and Abbatt, J. P. D.: Connecting the oxidation of soot to its redox cycling abilities, Nat. Commun., 6, 10.1038/ncomms7812, 2015.

Apicella, B., Barbella, R., Ciajolo, A., and Tregrossi, A.: Comparative analysis of the structure of carbon materials relevant in combustion, Chemosphere, 51, 1063-1069, http://dx.doi.org/10.1016/S0045-6535(02)00715-4, 2003.

Balakrishna, S., Lomnicki, S., McAvey, K. M., Cole, R. B., Dellinger, B., and Cormier, S. A.: Environmentally persistent free radicals amplify ultrafine particle mediated cellular oxidative stress and cytotoxicity, Part. Fibre Toxicol., 6, 10.1186/1743-8977-6-11, 2009.

Barlow, P. G., Clouter-Baker, A., Donaldson, K., MacCallum, J., and Stone, V.: Carbon black nanoparticles induce type II epithelial cells to release chemotaxins for alveolar macrophages, Part. Fibre Toxicol., 2, 11, 10.1186/1743-8977-2-11, 2005.

Baumgartner, J., Zhang, Y., Schauer, J. J., Huang, W., Wang, Y., and Ezzati, M.: Highway proximity and black carbon from cookstoves as a risk factor for higher blood pressure in rural China, Proc. Natl. Acad. Sci. USA, 111, 13229-13234, 10.1073/pnas.1317176111, 2014.

Brown, D. M., Donaldson, K., and Stone, V.: Effects of PM_{10} in human peripheral blood monocytes and J774 macrophages, Respir. Res. 5, doi:10.1186/1465-9921-5-29, 2004.

Cain, J. P., Gassman, P. L., Wang, H., and Laskin, A.: Micro-FTIR study of soot chemical composition-evidence of aliphatic hydrocarbons on nascent soot surfaces, Phys. Chem. Chem. Phys., 12, 5206-5218, 10.1039/b924344e, 2010.

Cappella, P., Gasparri, F., Pulici, M., and Moll, J.: Cell proliferation method: click chemistry based on brdu coupling for multiplex antibody staining, Curr. Protoc. Cy., 72, 7.34.31-17, 10.1002/0471142956.cy0734s72, 2015.

Cedervall, T., Lynch, I., Lindman, S., Berggård, T., Thulin, E., Nilsson, H., Dawson, K. A., and Linse, S.: Understanding the nanoparticle–protein corona using methods to quantify exchange rates and affinities of proteins for nanoparticles, Proc. Natl. Acad. Sci. USA, 104, 2050-2055, 10.1073/pnas.0608582104, 2007.

Charrier, J. G., and Anastasio, C.: On dithiothreitol (DTT) as a measure of oxidative potential for ambient particles: evidence for the importance of soluble transition metals, Atmos. Chem. Phys., 12, 9321-9333, 10.5194/acp-12-9321-2012, 2012.

Chen, D., He, D., Lu, J., Zhong, L., Liu, F., Liu, J., Yu, J., Wan, G., He, S., and Luo, Y.: Investigation of the role of surface lattice oxygen and bulk lattice oxygen migration of cerium-based oxygen carriers: XPS and designed H_2-TPR characterization, Appl. Catal. B: Environ., 218, 249-259, https://doi.org/10.1016/j.apcatb.2017.06.053, 2017.

Cho, A. K., Sioutas, C., Miguel, A. H., Kumagai, Y., Schmitz, D. A., Singh, M., Eiguren-Fernandez, A., and Froines, J. R.: Redox activity of airborne particulate matter at different sites in the Los Angeles Basin, Environ. Res., 99, 40-47, http://dx.doi.org/10.1016/j.envres.2005.01.003, 2005.

649 Cho, M.-H., Niles, A., uili Huang, Inglese, J., Austin, C. P., Riss, T., and Xia, M.: A bioluminescent
650 cytotoxicity assay for assessment of membrane integrity using a proteolytic biomarker, Toxicol. In Vitro.,
651 22, 1099-1106, 2008.
652 Corbin, J. C., Lohmann, U., Sierau, B., Keller, A., Burtscher, H., and Mensah, A. A.: Black carbon surface
653 oxidation and organic composition of beech-wood soot aerosols, Atmos. Chem. Phys., 15, 11885-11907,
654 10.5194/acp-15-11885-2015, 2015.
655 Dugas, T. R., Lomnicki, S., Cormier, S. A., Dellinger, B., and Reams, M.: Addressing emerging risks:
656 scientific and regulatory challenges associated with environmentally persistent free radicals, Int. J.
657 Environ. Res. Public Health, 13, 17, 10.3390/ijerph13060573, 2016.
658 Fang, T., Verma, V., Bates, J. T., Abrams, J., Klein, M., Strickland, M. J., Sarnat, S. E., Chang, H. H.,
659 Mulholland, J. A., Tolbert, P. E., Russell, A. G., and Weber, R. J.: Oxidative potential of ambient water-
660 soluble PM2.5 in the southeastern United States: contrasts in sources and health associations between
661 ascorbic acid (AA) and dithiothreitol (DTT) assays, Atmos. Chem. Phys., 16, 3865-3879, 10.5194/acp-
662 16-3865-2016, 2016.
663 Foroozandeh, P., and Aziz, A. A.: Insight into cellular uptake and intracellular trafficking of nanoparticles,
664 Nanoscale Res. Lett., 13, 339-339, 10.1186/s11671-018-2728-6, 2018.
665 Golberg, D., Costa, P., Wang, M. S., Wei, X. L., Tang, D. M., Xu, Z., Huang, Y., Gautam, U. K., Liu, B.
666 D., Zeng, H. B., Kawamoto, N., Zhi, C. Y., Mitome, M., and Bando, Y.: Nanomaterial engineering and
667 property studies in a transmission electron microscope, Adv. Mater., 24, 177-194,
668 10.1002/adma.201102579, 2012.
669 Gupta, P., Agrawal, A., Murali, K., Varshney, R., Beniwal, S., Manhas, S., Roy, P., and Lahiri, D.:
670 Differential neural cell adhesion and neurite outgrowth on carbon nanotube and graphene reinforced
671 polymeric scaffolds, Mater. Sci. Eng. C-Mater. Biol. Appl., 97, 539-551, 10.1016/j.msec.2018.12.065,
672 2019.
673 Hadrup, N., Bengtson, S., Jacobsen, N. R., Jackson, P., Nocun, M., Saber, A. T., Jensen, K. A., Wallin,
674 H., and Vogel, U.: Influence of dispersion medium on nanomaterial-induced pulmonary inflammation
675 and DNA strand breaks: investigation of carbon black, carbon nanotubes and three titanium dioxide
676 nanoparticles, Mutagenesis, 32, 581-597, 10.1093/mutage/gex042, 2017.
677 Han, C., Liu, Y., Liu, C., Ma, J., and He, H.: Influence of combustion conditions on hydrophilic properties
678 and microstructure of flame soot, J. Phys. Chem. A, 116, 4129-4136, 10.1021/jp301041w, 2012a.
679 Han, C., Liu, Y., Ma, J., and He, H.: Effect of soot microstructure on its ozonization reactivity, J. Chem.
680 Phys., 2012 http://dx.doi.org/10.1063/1.4747190, 2012b.
681 He, G., and He, H.: DFT studies on the heterogeneous oxidation of SO_2 by oxygen functional groups on
682 graphene, Phys. Chem. Chem. Phys., 18, 31691-31697, 2016.
683 Helland, A., Wick, P., Koehler, A., Schmid, K., and Som, C.: Reviewing the environmental and human
684 health knowledge base of carbon nanotubes, Environ. Health Perspect., 115, 1125-1131, 2007.
685 Holder, A. L., Carter, B. J., Goth–Goldstein, R., Lucas, D., and Koshland, C. P.: Increased cytotoxicity
686 of oxidized flame soot, Atmos. Pollu. Res. , 3, 25-31, 2012.
687 Hu, L., Hecht, D. S., and Grüner, G.: Carbon nanotube thin films: Fabrication, properties, and
688 applications, Chem. Rev., 110, 5790-5844, 10.1021/cr9002962, 2010.
689 Hunt, A., Dikin, D. A., Kurmaev, E. Z., Boyko, T. D., Bazylewski, P., Chang, G. S., and Moewes, A.:
690 Epoxide speciation and functional group distribution in graphene oxide paper-like materials, Adv. Funct.
691 Mater., 22, 3950-3957, 10.1002/adfm.201200529, 2012.
692 Inagaki, M., and Kang, F.: Materials science and engineering of carbon: Fundamentals (Second Edition),

693 Butterworth-Heinemann, Oxford, 542 pp., 2014.
694 Johnson, K. S., Zuberi, B., Molina, L. T., Molina, M. J., Iedema, M. J., Cowin, J. P., Gaspar, D. J., Wang,
695 C., and Laskin, A.: Processing of soot in an urban environment: case study from the Mexico City
696 Metropolitan Area, Atmos. Chem. Phys., 5, 3033-3043, 10.5194/acp-5-3033-2005, 2005.
697 Keshavan, S., Oropesa-Nunez, R., Diaspro, A., Canale, C., and Dante, S.: Adhesion and migration of
698 CHO cells on micropatterned single layer graphene, 2D Mater., 4, 9, 10.1088/2053-1583/aa57e9, 2017.
699 Kim, H., Park, K., and Lee, M.-Y.: Biocompatible dispersion methods for carbon black, Toxicol. Res.,
700 28, 209-216, 2012.
701 Koike, E., and Kobayashi, T.: Chemical and biological oxidative effects of carbon black nanoparticles,
702 Chemosphere, 65, 946-951, http://dx.doi.org/10.1016/j.chemosphere.2006.03.078, 2006.
703 Koromilas, N. D., Lainioti, G. C., Gialeli, C., Barbouri, D., Kouravelou, K. B., Karamanos, N. K.,
704 Voyiatzis, G. A., and Kallitsis, J. K.: Preparation and toxicological assessment of functionalized carbon
705 nanotube-polymer hybrids, Plos One, 9, 10.1371/journal.pone.0107029, 2014.
706 Kumagai, Y., Koide, S., Taguchi, K., Endo, A., Nakai, Y., Yoshikawa, T., and Shimojo, N. C.: Oxidation
707 of proximal protein sulfhydryls by phenanthraquinone, a component of diesel exhaust particles, Chem.
708 Res. Toxicol., , 15, 483-489, 2002.
709 Kumarathasan, P., Das, D., Salam, M. A., Mohottalage, S., DeSilva, N., Simard, B., and Vincent, R.:
710 Mass spectrometry-based proteomic assessment of the in vitro toxicity of carbon nanotubes, Curr. Topics
711 Biochem. Res., 14, 15-27, 2012.
712 Kumarathasan, P., Breznan, D., Das, D., Salam, M. A., Siddiqui, Y., MacKinnon-Roy, C., Guan, J., de
713 Silva, N., Simard, B., and Vincent, R.: Cytotoxicity of carbon nanotube variants: A comparative in vitro
714 exposure study with A549 epithelial and J774 macrophage cells, Nanotoxicology, 9, 148-161,
715 doi:10.3109/17435390.2014.902519, 2014.
716 Kumarathasan, P., Breznan, D., Das, D., Salam, M. A., Siddiqui, Y., MacKinnon-Roy, C., Guan, J., de
717 Silva, N., Simard, B., and Vincent, R.: Cytotoxicity of carbon nanotube variants: A comparative in vitro
718 exposure study with A549 epithelial and J774 macrophage cells, Nanotoxicology, 9, 148-161,
719 10.3109/17435390.2014.902519, 2015.
720 Kuznetsova, A., Popova, I., Yates, J. T., Bronikowski, M. J., Huffman, C. B., Liu, J., Smalley, R. E., Hwu,
721 H. H., and Chen, J. G.: Oxygen-containing functional groups on single-wall carbon nanotubes: nexafs
722 and vibrational spectroscopic studies, J. Am. Chem. Soc., 123, 10699-10704, 10.1021/ja011021b, 2001.
723 Lacerda, L., Ali-Boucetta, H., Kraszewski, S., Tarek, M., Prato, M., Ramseyer, C., Kostarelos, K., and
724 Bianco, A.: How do functionalized carbon nanotubes land on, bind to and pierce through model and
725 plasma membranes, Nanoscale, 5, 10242-10250, 10.1039/c3nr03184e, 2013.
726 Lam, J., Herant, M., Dembo, M., and Heinrich, V.: Baseline Mechanical characterization of J774
727 macrophages, Biophys. J., 96, 248-254, 2009.
728 Langley, L. A., Villanueva, D. E., and Fairbrother, D. H.: Quantification of surface oxides on
729 carbonaceous materials, Chem. Mater. , 18, 169-178, 2006.
730 Lara-Martinez, L. A., Masso, F., Gonzalez, E. P., Garcia-Pelaez, I., Contreras-Ramos, A., Valverde, M.,
731 Rojas, E., Cervantes-Sodi, F., and Hernandez-Gutierrez, S.: Evaluating the biological risk of
732 functionalized multiwalled carbon nanotubes and functionalized oxygen-doped multiwalled carbon
733 nanotubes as possible toxic, carcinogenic, and embryotoxic agents, Inter. J. Nanomed., 12, 7695-7707,
734 10.2147/ijn.s144777, 2017.
735 Lee, Y. S., Park, S. H., Lee, J. C., and Ha, K.: Influence of microstructure in nitrile polymer on curing
736 characteristics and mechanical properties of carbon black-filled rubber composite for seal applications,

J. Elastomer Plast., 48, 659-676, 10.1177/0095244315613621, 2016.
Li, N., Kim, S., Wang, M., Froines, J., Sioutas, C., and Nel, A.: Use of a stratified oxidative stress model to study the biological effects of ambient concentrated and diesel exhaust particulate matter, Inhal. Toxicol., 14, 459-486, 10.1080/08958370175367857l, 2002a.
Li, N., Wang, M., Oberley, T. D., Sempf, J. M., and Nel, A. E.: Comparison of the pro-oxidative and proinflammatory effects of organic diesel exhaust particle chemicals in bronchial epithelial cells and macrophages, J. Immunol., 169, 4531-4541, 2002b.
Li, N., Sioutas, C., Cho, A., Schmitz, D., Misra, C., Sempf, J., Wang, M., Oberley, T., Froines, J., and Nel, A.: Ultrafine particulate pollutants induce oxidative stress and mitochondrial damage, Environ. Health Perspect., 111, 455-460, 2003.
Li, Q., Wyatt, A., and Kamens, R. M.: Oxidant generation and toxicity enhancement of aged-diesel exhaust, Atmos. Environ., 43, 1037-1042, http://dx.doi.org/10.1016/j.atmosenv.2008.11.018, 2009.
Li, Q., Shang, J., and Zhu, T.: Physicochemical characteristics and toxic effects of ozone-oxidized black carbon particles, Atmos. Environ., 81, 68-75, http://dx.doi.org/10.1016/j.atmosenv.2013.08.043, 2013.
Li, Q., Shang, J., Liu, J., Xu, W., Feng, X., Li, R., and Zhu, T.: Physicochemical characteristics, oxidative capacities and cytotoxicities of sulfate-coated, 1,4-NQ-coated and ozone-aged black carbon particles, Atmos. Res., 153, 535-542, http://dx.doi.org/10.1016/j.atmosres.2014.10.005, 2015.
Li, R. B., Guiney, L. M., Chang, C. H., Mansukhani, N. D., Ji, Z. X., Wang, X., Liao, Y. P., Jiang, W., Sun, B. B., Hersam, M. C., Nel, A. E., and Xia, T.: Surface oxidation of graphene oxide determines membrane damage, lipid peroxidation, and cytotoxicity in macrophages in a pulmonary toxicity model, ACS Nano, 12, 1390-1402, 10.1021/acsnano.7b07737, 2018.
Liu, Q., Baumgartner, J., Zhang, Y., Liu, Y., Sun, Y., and Zhang, M.: Oxidative potential and inflammatory impacts of source apportioned ambient air pollution in beijing, Environ. Sci. Technol., 48, 12920-12929, 10.1021/es5029876, 2014a.
Liu, Q., Liggio, J., Breznan, D., Thomson, E. M., Kumarathasan, P., Vincent, R., Li, K., and Li, S.-M.: Oxidative and toxicological evolution of engineered nanoparticles with atmospherically relevant coatings, Environ. Sci. Technol., 53, 3058-3066, 10.1021/acs.est.8b06879, 2019.
Liu, Y., Liu, C., Ma, J., Ma, Q., and He, H.: Structural and hygroscopic changes of soot during heterogeneous reaction with O_3, Phys. Chem. Chem. Phys., 12, 10896-10903, 2010.
Liu, Y., Ai, K., and Lu, L.: Polydopamine and its derivative materials: synthesis and promising applications in energy, environmental, and biomedical fields, Chem. Rev., 114, 5057-5115, 10.1021/cr400407a, 2014b.
Liu, Y., Liggio, J., Li, S.-M., Breznan, D., Vincent, R., Thomson, E. M., Kumarathasan, P., Das, D., Abbatt, J., Antiñolo, M., and Russell, L.: Chemical and toxicological evolution of carbon nanotubes during atmospherically relevant aging processes, Environ. Sci. Technol., 49, 2806-2814, 10.1021/es505298d, 2015.
Long, C. M., Nascarella, M. A., and Valberg, P. A.: Carbon black vs. black carbon and other airborne materials containing elemental carbon: Physical and chemical distinctions, Environ. Pollut., 181, 271-286, http://dx.doi.org/10.1016/j.envpol.2013.06.009, 2013.
Maruyama, T.: Current status of single-walled carbon nanotube synthesis from metal catalysts by chemical vapor deposition, Mater. Express, 8, 1-20, 10.1166/mex.2018.1407, 2018.
Mawhinney, D. B., Naumenko, V., Kuznetsova, A., Yates, J. T., Liu, J., and Smalley, R. E.: Infrared spectral evidence for the etching of carbon nanotubes: Ozone oxidation at 298 K, J. Am. Chem. Soc., 122, 2383-2384, 10.1021/ja994094s, 2000.

McWhinney, R. D., Badali, K., Liggio, J., Li, S.-M., and Abbatt, J. P. D.: Filterable redox cycling activity: a comparison between diesel exhaust particles and secondary organic aerosol constituents, Environ. Sci. Technol., 47, 3362-3369, 10.1021/es304676x, 2013a.

McWhinney, R. D., Zhou, S., and Abbatt, J. P. D.: Naphthalene SOA: redox activity and naphthoquinone gas–particle partitioning, Atmos. Chem. Phys., 13, 9731-9744, 10.5194/acp-13-9731-2013, 2013b.

Muckenhuber, H., and Grothe, H.: The heterogeneous reaction between soot and NO_2 at elevated temperature, Carbon 44, 546-559, 2006.

Nel, A., Xia, T., Määdler, L., and Li, N.: Toxic potential of materials at the nanolevel., Science, 311, 622-627, 2006.

Nienow, A. M., and Roberts, J. T.: Heterogeneos chemsitry of carbon aerosols, Annu. Rev. Phys. Chem., 57, 105-128, 2006.

Niranjan, R., and Thakur, A. K.: The toxicological mechanisms of environmental soot (black carbon) and carbon black: Focus on oxidative stress and inflammatory pathways, Front. Immunol., 8, 20, 10.3389/fimmu.2017.00763, 2017.

Parant, H., Muller, G., Le Mercier, T., Tarascon, J. M., Poulin, P., and Colin, A.: Flowing suspensions of carbon black with high electronic conductivity for flow applications: Comparison between carbons black and exhibition of specific aggregation of carbon particles, Carbon, 119, 10-20, 10.1016/j.carbon.2017.04.014, 2017.

Peebles, B. C., Dutta, P. K., Waldman, W. J., Villamena, F. A., Nash, K., Severance, M., and Nagy, A.: Physicochemical and toxicological properties of commercial carbon blacks modified by reaction with ozone, Environ. Sci. Technol., 45, 10668-10675, 2011.

Peng, J., Hu, M., Guo, S., Du, Z., Zheng, J., Shang, D., Levy Zamora, M., Zeng, L., Shao, M., Wu, Y.-S., Zheng, J., Wang, Y., Glen, C. R., Collins, D. R., Molina, M. J., and Zhang, R.: Markedly enhanced absorption and direct radiative forcing of black carbon under polluted urban environments, Proc. Natl. Acad. Sci. USA, 113, 4266-4271, 10.1073/pnas.1602310113, 2016.

Popovicheva, O. B., Kireeva, E. D., Shonija, N. K., Vojtisek-Lom, M., and Schwarz, J.: FTIR analysis of surface functionalities on particulate matter produced by off-road diesel engines operating on diesel and biofuel, Environ. Sci. Pollut. Res., 22, 4534-4544, 10.1007/s11356-014-3688-8, 2015.

Sanders, I. J., and Peeten, T. L.: Carbon black: Production, Properties and uses, Chemical engineering methods and technology Materials Science and Technologies Series, Nova Science Publishers, UK, 2011.

Schuster, M. E., Hävecker, M., Arrigo, R., Blume, R., Knauer, M., Ivleva, N. P., Su, D. S., Niessner, R., and Schlögl, R.: Surface sensitive study to determine the reactivity of soot with the focus on the european emission standards IV and VI, J. Phys. Chem. A., 115, 2568-2580, 10.1021/jp1088417, 2011.

Shvedova, A. A., Pietroiusti, A., Fadeel, B., and Kagan, V. E.: Mechanisms of carbon nanotube-induced toxicity: Focus on oxidative stress, Toxicol. Appl. Pharmacol., 261, 121-133, 2012.

Simmons, J. M., Nichols, B. M., Baker, S. E., Marcus, M. S., Castellini, O. M., Lee, C. S., Hamers, R. J., and Eriksson, M. A.: Effect of ozone oxidation on single-walled carbon nanotubes, J. Phys. Chem. B, 110, 7113-7118, 10.1021/jp0548422, 2006.

Somiya, S.: Handbook of advanced ceramics : Materials, application, processing, and properties, 2nd ed., Academic Press, 2013.

Tiwari, A. J., and Marr, L. C.: The role of atmospheric transformations in determing envrionmental impacts of carbonaceous nanoparticles, J. Environ. Qual., 39, 1883-1895, 2010.

Truong, H., Lomnicki, S., and Dellinger, B.: Potential for misidentification of environmentally persistent free radicals as molecular pollutants in particulate matter, Environ. Sci. Technol., 44, 1933-1939,

825 10.1021/es902648t, 2010.
826 Wal, R. L. V., Bryg, V. M., and Hays, M. D.: XPS Analysis of combustion aerosols for chemical
827 composition, surface chemistry, and carbon chemical state, Anal. Chem., 83, 1924-1930,
828 10.1021/ac102365s, 2011.
829 Wang, B., Li, K., Jin, W., Lu, Y., Zhang, Y., Shen, G., Wang, R., Shen, H., Li, W., Huang, Y., Zhang, Y.,
830 Wang, X., Li, X., Liu, W., Cao, H., and Tao, S.: Properties and inflammatory effects of various size
831 fractions of ambient particulate matter from beijing on A549 and J774A.1 Cells, Environ. Sci. Technol.,
832 47, 10583-10590, 10.1021/es401394g, 2013.
833 WHO: World Health Organization. Health effects of particulate matter: Policy implications for countries
834 in eastern Europe, Caucasus and central Asia, 2013.
835 Xia, T., Kovochich, M., Brant, J., Hotze, M., Sempf, J., Oberley, T., Sioutas, C., Yeh, J. I., Wiesner, M.
836 R., and Nel, A. E.: Comparison of the abilities of ambient and manufactured nanoparticles to induce
837 cellular toxicity according to an oxidative stress paradigm, Nano Lett., 6, 1794-1807, 10.1021/nl061025k,
838 2006.
839 Yim, W. L., and Johnson, J. K.: Ozone oxidation of single walled carbon nanotubes from density
840 functional theory, J. Phys. Chem. C, 113, 17636-17642, 10.1021/jp908089c, 2009.
841 Zhang, B., Wei, P., Zhou, Z., and Wei, T.: Interactions of graphene with mammalian cells: Molecular
842 mechanisms and biomedical insights, Adv. Drug Deliv. Rev., 105, 145-162,
843 https://doi.org/10.1016/j.addr.2016.08.009, 2016.
844 Zhang, X., Wang, S., Xu, L., Feng, L., Ji, Y., Tao, L., Li, S., and Wei, Y.: Biocompatible polydopamine
845 fluorescent organic nanoparticles: facile preparation and cell imaging, Nanoscale, 4, 5581-5584,
846 10.1039/c2nr31281f, 2012.

847

848

849 **Figure captions**

850 **Figure 1**. DTT decay rates of several black carbon materials compared with literature
851 results (Li et al., 2013;Charrier and Anastasio, 2012;Liu et al., 2014a;Li et al., 2015;Liu
852 et al., 2015;Holder et al., 2012;Antinolo et al., 2015).

853 **Figure 2**. Cytotoxicity of (A) SB4A, (B) graphene, (C) graphene oxide, (D) SWCNT,
854 (E) SWCNT-OH and (F) SWCNT-COOH toward murine J774 cell line. The stars mean
855 the difference is significant at 0.05 level for a certain dose of carbon nanomaterials
856 compared with the corresponding blank experiments.

857 **Figure 3**. (A) Thermo gravity curves of carbon nanomaterials in nitrogen gas flow;
858 (B) the corresponding differential thermal analysis curves. The insert graph shows the
859 weight loss due to desorption of organics.

860 **Figure 4**. XPS spectra of carbon nanomaterials. (A)-(F) are O1s spectra and (G)-(L)
861 are C1s spectra for SB4A, graphene, graphene oxide, SWCNT, SWCNT-OH and
862 SWCNT-COOH, respectively.

863 **Figure 5**. (A) Distribution of oxygen containing species on the tested carbon
864 nanomaterials; (B) comparison of oxygen-containing species and (C) DTT decay rate
865 between graphene oxide and other carbon nanomaterials.

866 **Figure 6.** DTT decay rate for graphene oxide and thermally treated graphene oxide in N_2 flow
867 at 200 °C.
868

869 **Figures**

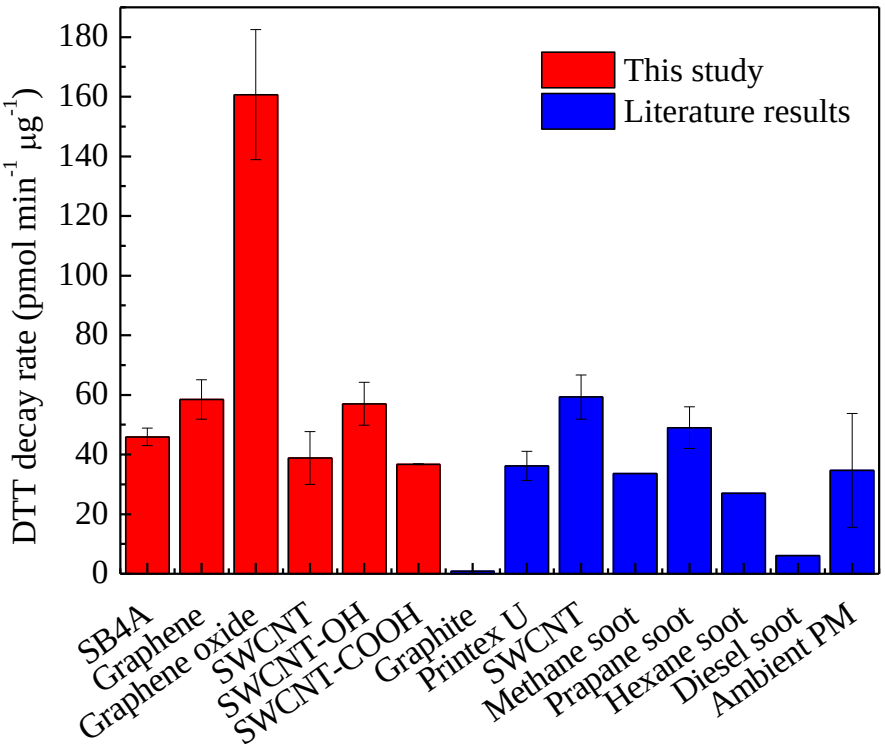

870

871 Fig. 1

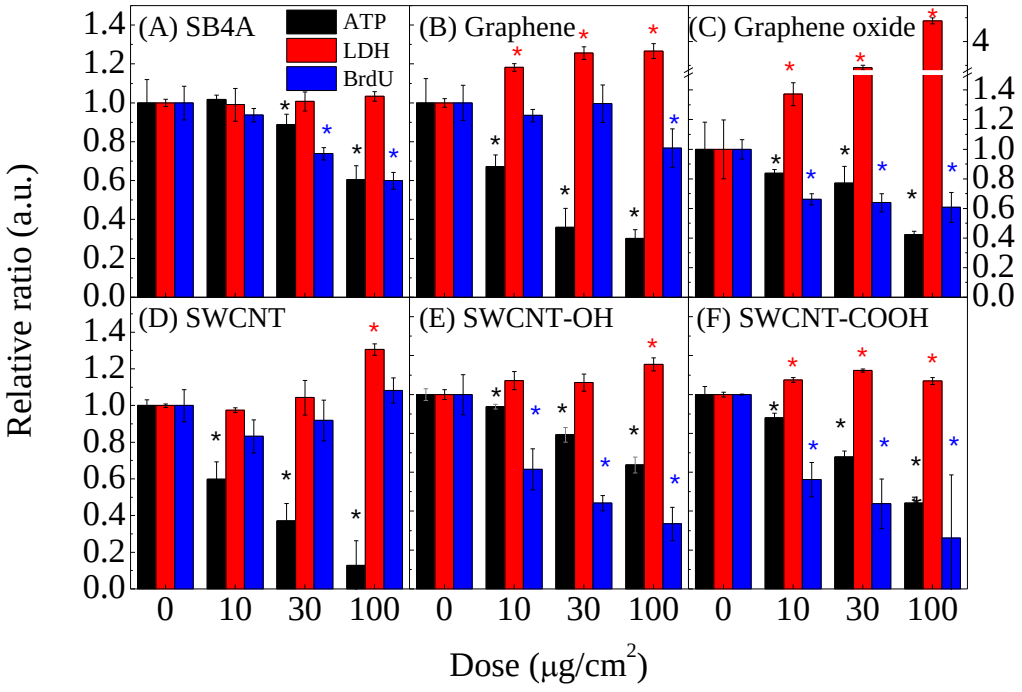

872

873 Fig. 2

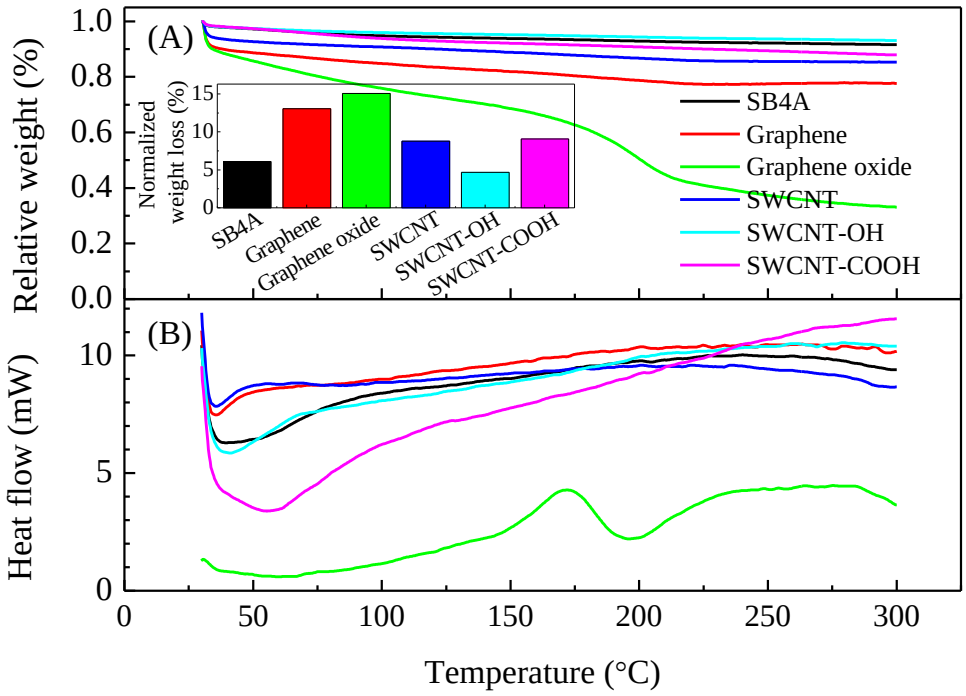

874

875 Fig. 3.

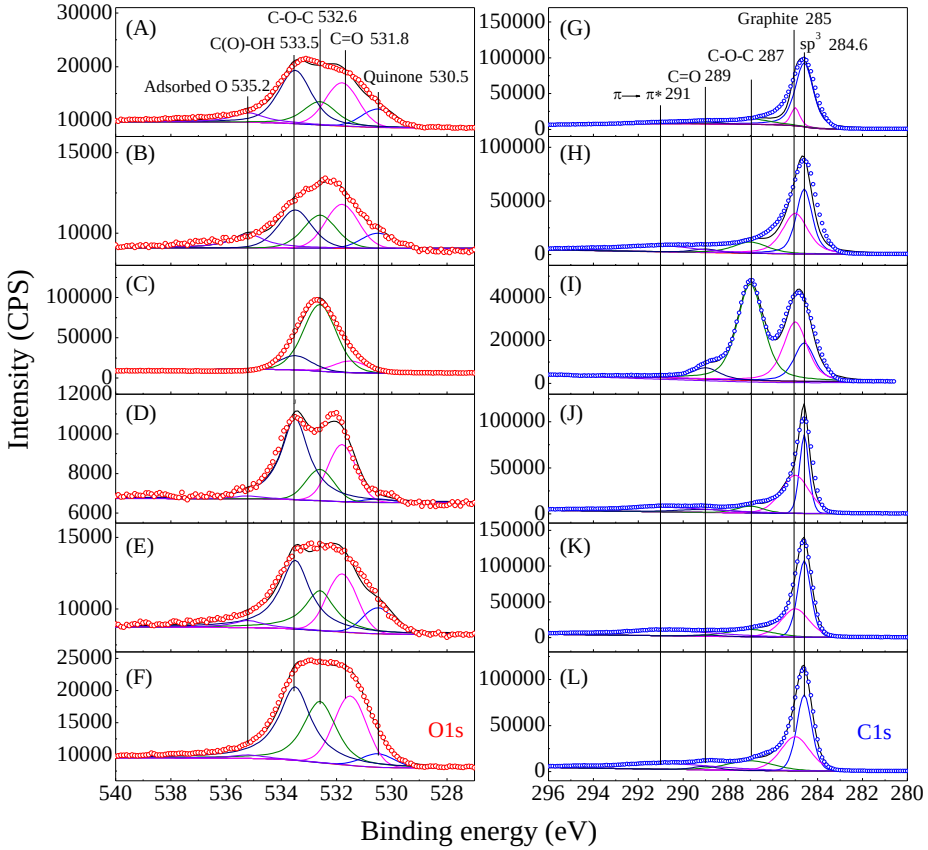

876

877 Fig. 4.

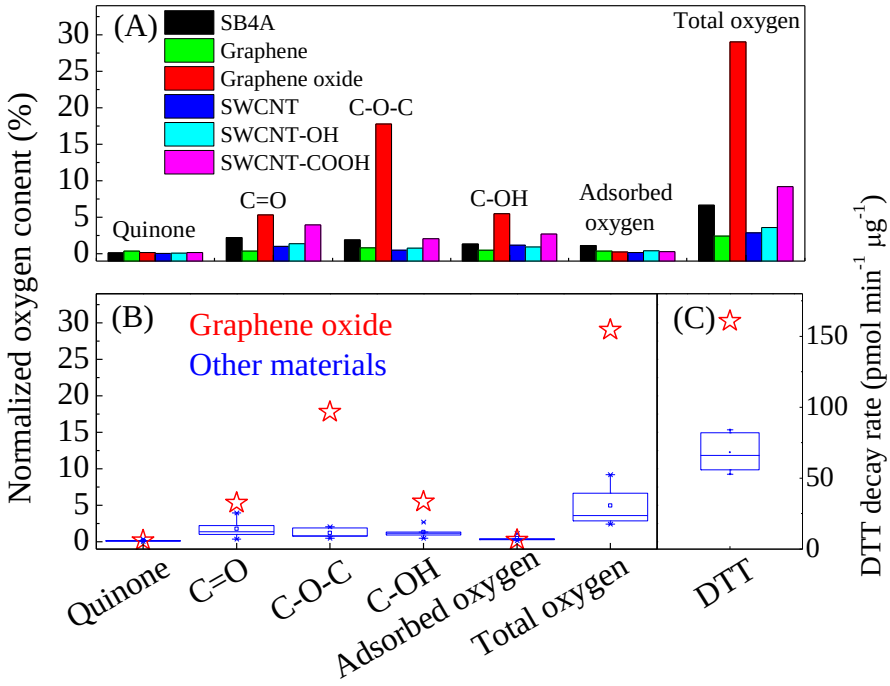

878

879 Fig. 5.

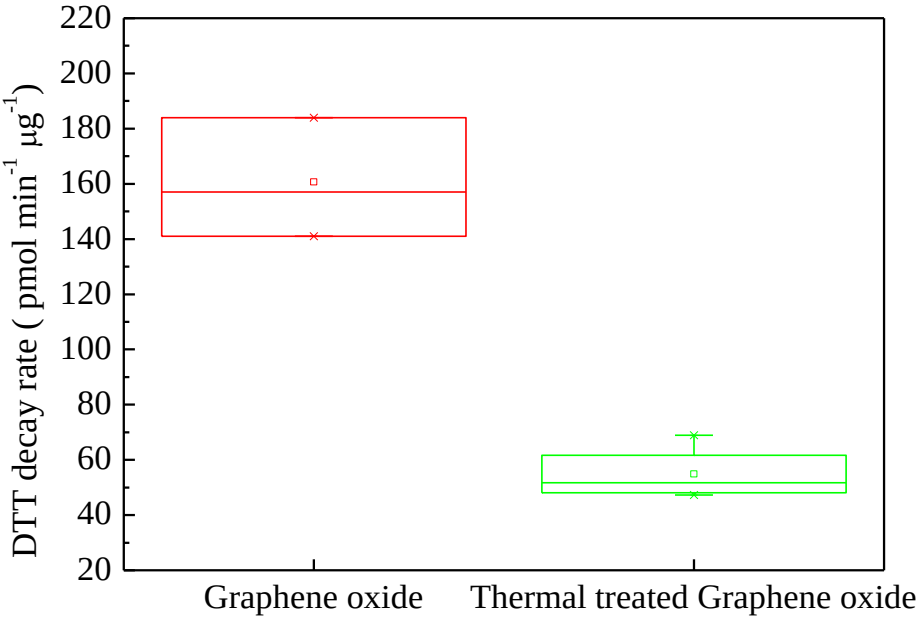

880

881 Figure 6.

882